Theoretical investigation of dephosphorylation of phosphate monoesters on CeO_2(111)

Chuanlin Zhao and Ye Xu*

Cain Department of Chemical Engineering, Louisiana State University, Baton Rouge, LA 70803, USA

Abstract

The dephosphorylation of neutral model phosphate monoesters on CeO_2(111), including *para*-nitrophenyl phosphate and methyl phosphate, has been studied theoretically using self-consistent, periodic density functional theory calculations at the GGA+U-PW91 level. These phosphate monoesters interact strongly with CeO_2(111) by forming a bond between the P atom and a surface lattice O atom. A surface-assisted hydrolysis mechanism is proposed for the catalytic dephosphorylation of the phosphate monoesters on CeO_2(111), which involves P-O ester bond scission followed by phosphate hydration and product desorption. The energies of the transition states for the P-O ester bond scission are found to follow a linear scaling relation with respect to the energies of the dissociated fragments reasonably well. A nearly spontaneous transfer of one of the H atoms on the phosphate group to the alkoxide group produces the corresponding alcohol. The hydration of the remaining HPO_3 group has a maximum activation energy of ca. 1.1 eV *in vacuo*. Thus although the nature of the alkoxide group affects the activation of the P-O ester bond, it should not affect the overall catalytic activity of CeO_2(111) for dephosphorylation because the hydration of the phosphate group is rate-limiting.

Keywords Ceria · Dephosphorylation · Organophosphates · *Para*-nitrophenyl phosphate · Oxide catalysis · DFT

1 Introduction

Phosphorous (P) serves as an essential building block for life on earth, and is critical for food production. Thus, it has a huge impact on the stability and prosperity of human societies [1]. With the steady growth of global population, primary phosphorus fertilizers necessary for high crop yields have transitioned from animal wastes to mined phosphate rock, i.e., phosphorite. However, phosphorite is a nonrenewable resource and is distributed quite unevenly from a geographic perspective, and high-grade phosphorite sources are declining [2]. On the other hand, agricultural runoff, industrial wastewater, and human sewage often contains significant amounts of phosphates, which are in part responsible for eutrophication that creates hypoxic dead zones in waterbodies close to shorelines that threatens aquaculture industries but also jeopardizes potable water resources [3]. Furthermore, organophosphates (OPs), which are found in many consumer, industrial, and agricultural chemical products, often possess toxicity to animals and even humans. Removal of P from wastewater as well as extraction of P from biomass feedstock constitutes important steps in sustainable P use [4]. Environmental necessity and economic and technological feasibility of such methods suggest that the further development of and support for sustainable P use need to be on the agenda of policymakers today [5].

The degradation of OPs in the environment can take months and even years [6, 7]. The hydrolysis of the P-O ester bond by microbes is the primary pathway for OP degradation in nature [8]. Earlier studies have demonstrated promising catalytic activities of cerium oxide nanoparticles toward aqueous-phase dephosphorylation, i.e. hydrolysis, of organic and biological compounds including phosphopeptides, *para*-nitrophenyl phosphate (*p*-NPP), ATP, and phospho-tyrosine [9, 10] that parallel the function of phosphatases. Recently, Janos et al. suggested that ceria-based reactive sorbents can promote the dephosphorylation of several OP

pesticides and chemical warfare agents, which opens up a new frontier for ceria in environmental catalysis and may be relevant to large-scale environmental application of P recovery technologies [11, 12]. Manto et al. very recently studied the catalytic dephosphorylation of *p*-NPP using different ceria nano-shapes, among which nano-spheres (ca. 4 nm; no preferential exposed facet) showed the highest catalytic activity, followed by nano-octahedra (ca. 18 nm), which primarily expose (111) facets [13]. Although extensive experimental and theoretical studies have been reported in the literature that examine the hydrolysis mechanism of phosphate esters in aqueous solutions or by enzymatic complexes [14-21], the understanding of the dephosphorylation process on solid surfaces remains incomplete [22-26].

Here we report a DFT+U study on the dephosphorylation of model phosphate monoesters, including *p*-NPP and methyl phosphate (MP), on CeO_2(111) *in vacuo* in order to shed light on the factors controlling the kinetics of this reaction and to help establish the range of OPs the dephosphorylation of which ceria may effectively catalyze under mild or ambient conditions. The OPs are modeled in their neutral forms ($PO(OH)_2OR$) in this work, e.g. *p*-NPP-H_2 and MP-H_2, which are the predominant forms in acidic to neutral conditions [15, 27]. The deprotonated forms (i.e., the mono-anionic *p*-NPP-H_1/MP-H_1 and di-anionic *p*-NPP-H_0/MP-H_0) that prevail in neutral to basic solutions [28] will be considered in a future study. The dephosphorylation of *p*-NPP is of interest because it is accompanied by visible color change of the solution, which allows the reaction kinetics to be readily analyzed using ultraviolet-visible (UV-Vis) absorption spectroscopy [13]. By comparison, MP is the simplest organic phosphate monoester and is used here to explore how the leaving group affects the activation of the P-O ester bond. Moreover, a linear transition state scaling relation is proposed after considering several additional organic phosphate monoesters, including *para*-chlorophenyl phosphate (*p*-

ClPP), phenyl phosphate (*p*-HPP), 2-pyridyl phosphate (2-py-P), and chloro-methyl phosphate (Cl-MP). The formation and desorption of the resulting alcohol species (i.e. *para*-nitrophenol (*p*-NP) or 4-nitrophenol from *p*-NPP, and methanol from MP) are facile and therefore kinetically insignificant. On the other hand, the hydration and desorption of the remaining phosphate group are characterized by activation barriers of ca. 1.1 eV, although they may be reduced in aqueous phase. Our findings thus suggest that the nature of the leaving group should not have a strong impact on the kinetics of dephosphorylation of phosphate monoesters when catalyzed by ceria.

2 Methods

Periodic, spin-polarized DFT calculations were performed using the Vienna Ab initio Simulation Package (VASP) [29] in the generalized gradient approximation (GGA) using the Perdew-Wang (PW91) exchange-correlation functional [30]. The projector-augmented wave method (PAW) was used to describe the core electrons [31], and the Kohn–Sham valence states [Ce(5s5p4f5d6s), Cl(3s3p), P(3s3p), O(2s2p), N(2s2p), C(2s2p), H(1s)] were expanded in a plane wave basis set with a kinetic energy cutoff of 400 eV.

Gas-phase molecules or radicals were optimized in a neutral state in a 15×15×15 $Å^3$ simulation cell, which has been tested to be sufficiently large for the total energy of *p*-NPP to converge (the minimum-energy gas-phase structures for *p*-NPP and MP are shown in **Figure 1**). Dipole decoupling [32] was applied in all three lattice vector directions, and the reciprocal space was sampled at the Γ point only. Gas phase bond energies were calculated as $E_b^{\text{A-B}} = E_{AB} - E_A - E_B$, where AB, A, and B denotes the parent molecule itself and the corresponding dissociated fragments, respectively.

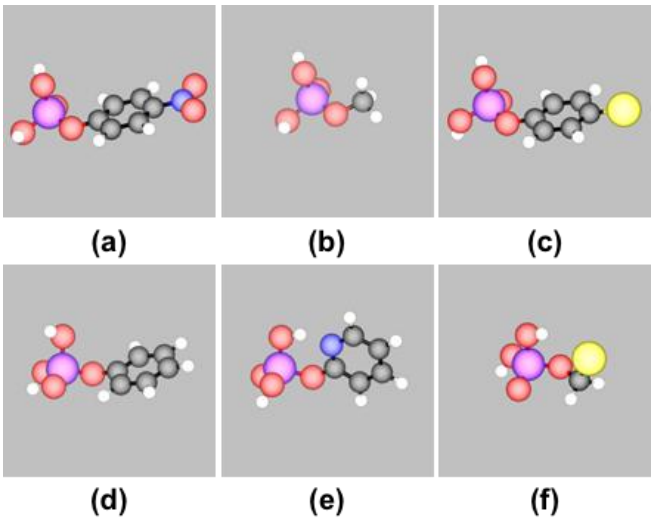

Figure 1. DFT-calculated minimum-energy gas-phase geometries for: (a) *para*-nitrophenyl phosphate (*p*-NPP); (b) methyl phosphate (MP); (c) *para*-chlorophenyl phosphate (*p*-ClPP); (d) phenyl phosphate (PP); (e) 2-pyridyl phosphate (2-py-P); (f) chloro-methyl phosphate (Cl-MP). Color code: red=O, violet=P, black=C, blue=N, white=H, and yellow=Cl.

The CeO_2(111) surface, which is thermodynamically the most stable facet of ceria, was modeled with a slab consisting of three O-Ce-O tri-layers with a p(3×3) surface unit cell, which corresponds to 1/9 monolayer (ML) coverage for one adsorbate per unit cell. The slab was separated from its periodic images in the *z* direction by ca. 12 Å of vacuum. A Γ-centered 2×2×1 Monkhorst-Pack k-point grid was used to sample the surface Brillouin zone [33]. Adsorption was studied only on one side of the slab, with dipole decoupling in the *z* direction. The top tri-layer of the slab and adsorbate were fully relaxed, and the remaining two tri-layers were fixed at the bulk positions. The adsorption energy of an atom or molecule was calculated as $\Delta E_{ads} = E_{total} - E_{slab} - E_{gas}$, where E_{total}, E_{slab} and E_{gas} refer to the energy of the slab with the adsorbed atom or molecule, the energy of the clean surface, the molecule or radical in the gas phase, respectively. Thus, the more negative the value of ΔE_{ads} is, the stronger the adsorption. The activation energy barrier was calculated as $E_a = E_{TS} - E_{IS}$, where E_{TS}, E_{IS} refer to the energy of transition and initial

state of the elementary step, respectively. If not specified, all activation energy barriers reported in this work include zero-point energy correction.

The minimum energy reaction path for each proposed elementary step and the associated transition state (TS) were determined using the climbing-image nudged elastic band method [34, 35] and dimer method [36, 37]. Geometry optimization and transition state search were converged to the extent that the maximum residual force was 0.03 eV/Å and 0.01 eV/Å or less in all relaxed degrees of freedom, respectively. Singlet-triplet/doublet-quadruplet splitting was checked, and the lower adsorption energy for an adsorbate and the lower activation energy for an elementary reaction step (at constant spin) are reported below. Vibrational modes and frequencies were calculated to determine zero point energies (ZPE) and to verify that each transition state possessed only one vibrational mode with a negative curvature in the direction of the bond breaking or forming process. A finite difference approximation approach of the dynamical matrix was used with a displacement of 0.01 Å. Very soft modes below 50 cm^{-1} were replaced with 50 cm^{-1} in calculating ZPEs.

The DFT+U formalism of Dudarev et al. [38] was used to partially offset the 4f electron delocalization error in DFT at the GGA level [39]. A U value of 2 eV was used based on our previous studies of surface reactions of organic oxygenates on CeO_2(111) [40-42]. The equilibrium lattice constant of the CeO_2 bulk was calculated to be 5.476 Å on a (15×15×15) Monkhorst-Pack k-point grid at U=2 eV, in close agreement with previous experimental and computational values [43]. Solvation energies of isolated molecules were estimated using the implicit solvation model implemented in VASPsol [44].

3 Results and Discussion

In the following, we present and discuss a surface-assisted hydrolysis mechanism for the dephosphorylation of *p*-NPP. The main surface intermediates involved in this mechanism will be presented first, and then the mechanism and its energy profile, which starts with the adsorption of *p*-NPP, followed by the P-O ester bond scission, the formation and desorption of *p*-NP, the hydration of the remaining phosphate group, and finally the desorption of phosphoric acid (H_3PO_4). Then a similar pathway is proposed and investigated for MP. Finally, a linear transition state scaling plot is presented for the activation of the P-O ester bond on CeO_2(111) for several additional organic monophosphates together with *p*-NPP and MP.

3.1 Molecular adsorption of p-NPP

Several geometries for molecular adsorption of neutral *p*-NPP are considered, and the minimum-energy configuration (**Figure 2a**) involves the formation of a P-O bond between the P atom and a lattice O atom (O_{latt}) in the surface with a bond length of 1.687 Å (summarized in **Table 1**), while the P-O ester bond is lengthened from 1.619 Å in the gas phase to 1.706 Å (see **Table 2**). The two acidic H atoms are attached to the axial O atom and one of the equatorial O atoms of the phosphate group, respectively. The three equatorial O atoms of the phosphate group are each located on a threefold hollow site above a Ce atom in the 2nd layer (designated as a $3f_c$ site, cf. **Figure 2b**). The minimum-energy configuration therefore involves a pentavalent P center with a weakened P-O ester bond and its formation is determined to be barrier-less. The adsorption energy of this adsorption state is -1.04 eV. It is 0.77 eV less stable for both of the acidic H atoms to be attached to equatorial O atoms instead (i.e., with the phosphoryl O atom (P=O) pointing away from surface). Another configuration that we have investigated involves *p*-NPP coordinated to a $3f_c$ site via the phosphoryl O at an O-Ce distance of 2.678 Å, similar to the

adsorption modes that previous theoretical studies of phosphate adsorption on oxides have considered [10, 28]. This configuration is calculated to be 0.74 eV less stable than the minimum-energy configuration.

Table 1. DFT-calculated minimum adsorption energies (ΔE_{ads}, in eV) and corresponding P-O bond lengths (d(P-O_{latt}), in Å), Bader[a] charges (in *e*) of the P atom and the O_{latt} atom beneath it, and magnetic moments of the systems (m.m., in μ_B).

Adsorbate	ΔE_{ads}	d(P-O_{latt})	*e*(P)	*e*(O_{latt})	m.m.
p-NPP	-1.04	1.687	+3.51	-1.34	0
MP	-1.04	1.701	+3.44	-1.31	0
p-NP_x[b]	-0.22	–	–	–	1
p-NP[b]	-0.42	–	–	–	0
CH_3O	-0.63	–	–	–	1
CH_3OH	-0.52	–	–	–	0
HPO_3	-3.02	1.594	+3.54	-1.43	0
H_2PO_3	-3.34	1.546	+3.58	-1.47	1
H_2PO_4	-1.18	1.785	+3.51	-1.13	1
H_3PO_4	-1.15	1.692	+3.50	-1.33	0

Adsorption energies are not zero-point energy-corrected. Adsorbate coverage is 1/9 ML. O_{latt} refers to the surface O atom that forms a bond with P.

[a] Bader charge partition analysis was performed using the approach of Henkelman [45], and the difference between the normal valence charge (6 for O and 5 for P) and Bader charge is reported herein. For comparison, the charge of O_{latt} in bulk CeO_2 is -1.22; the charge of P in gas phase *p*-NPP and MP is +3.55 and +3.56, respectively.

[b] *p*-NP_x: *para*-nitrophenoxide; *p*-NP: *para*-nitrophenol.

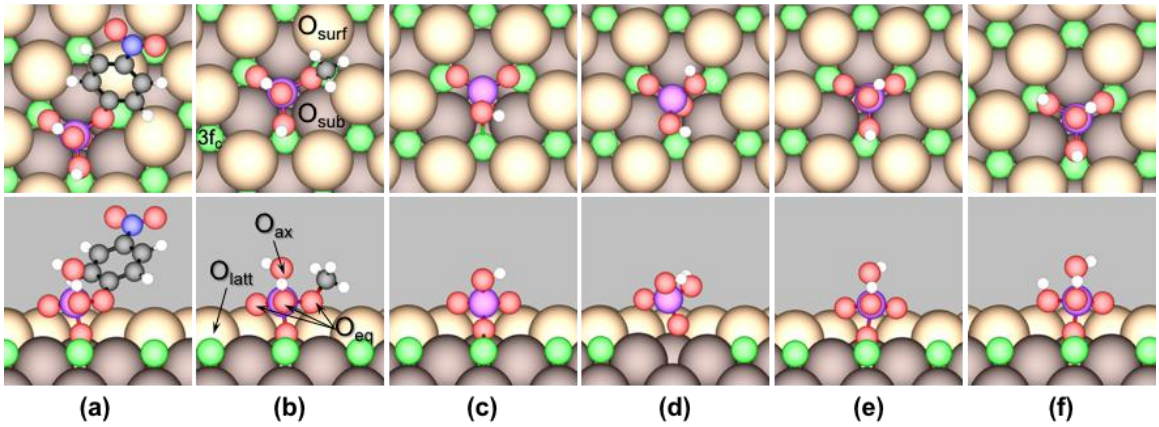

Figure 2. Top (top panels) and side (bottom panels) views of DFT-calculated minimum-energy geometries of (a) *p*-NPP, (b) MP, (c) HPO_3, (d) H_2PO_3, (e) H_2PO_4, and (f) H_3PO_4 adsorbed on CeO_2(111). In each panel, top view is on top and side view is on bottom. Color code: green=Ce, light brown=surface O_{latt},, dark brown=subsurface O_{latt}, red=O, violet=P, black=C, blue=N, and white=H. O_{ax}, O_{eq}, and O_{latt} refer to O atom at the axial, equatorial, and lattice position, respectively. Molecular images in this figure and those below are created using VESTA [46], with various bonds drawn for purpose of illustration only, and periodic images of the adsorbates removed for clarity; same below. The coordinates of these structures are reported in Supplemental Information.

3.2 Dephosphorylation of p-NPP

The calculated reaction energy profile for the proposed surface-assisted dephosphorylation mechanism for *p*-NPP is shown in **Figure 3**. The mechanism begins with the P-O ester bond scission, which begins with the H atom on the axial O atom of the phosphate group rotates to a position where it can form a hydrogen bond with the O atom of the *p*-NP_x group (*para*-nitrophenoxide or 4-nitrophenoxide) and stabilize the *p*-NP_x group once it is dissociated from the molecule. The P-O bond is further lengthened to 1.858 Å in the transition state (TS, shown in **Figure 3iii**). The activation barrier relative to the adsorbed *p*-NPP is a mere 0.13 eV (0.12 eV ZPE-corrected). Once the P-O ester bond is cleaved, the axial H atom on the dissociated H_2PO_3 group is transferred to *p*-NP_x to form *p*-NP (**Figure 3iv**). The *p*-NP presumably desorbs first due to weaker adsorption (ΔE_{ads} = -0.42 eV by itself, or -0.40 eV while co-adsorbed with the HPO_3 group). The remaining HPO_3 group then re-arranges itself to adopt the minimum-energy

configuration that occupies two $3f_c$ sites (**Figure 3v)**. Both the hydrogen transfer step and the HPO_3 re-arrangement step are found to be barrier-less.

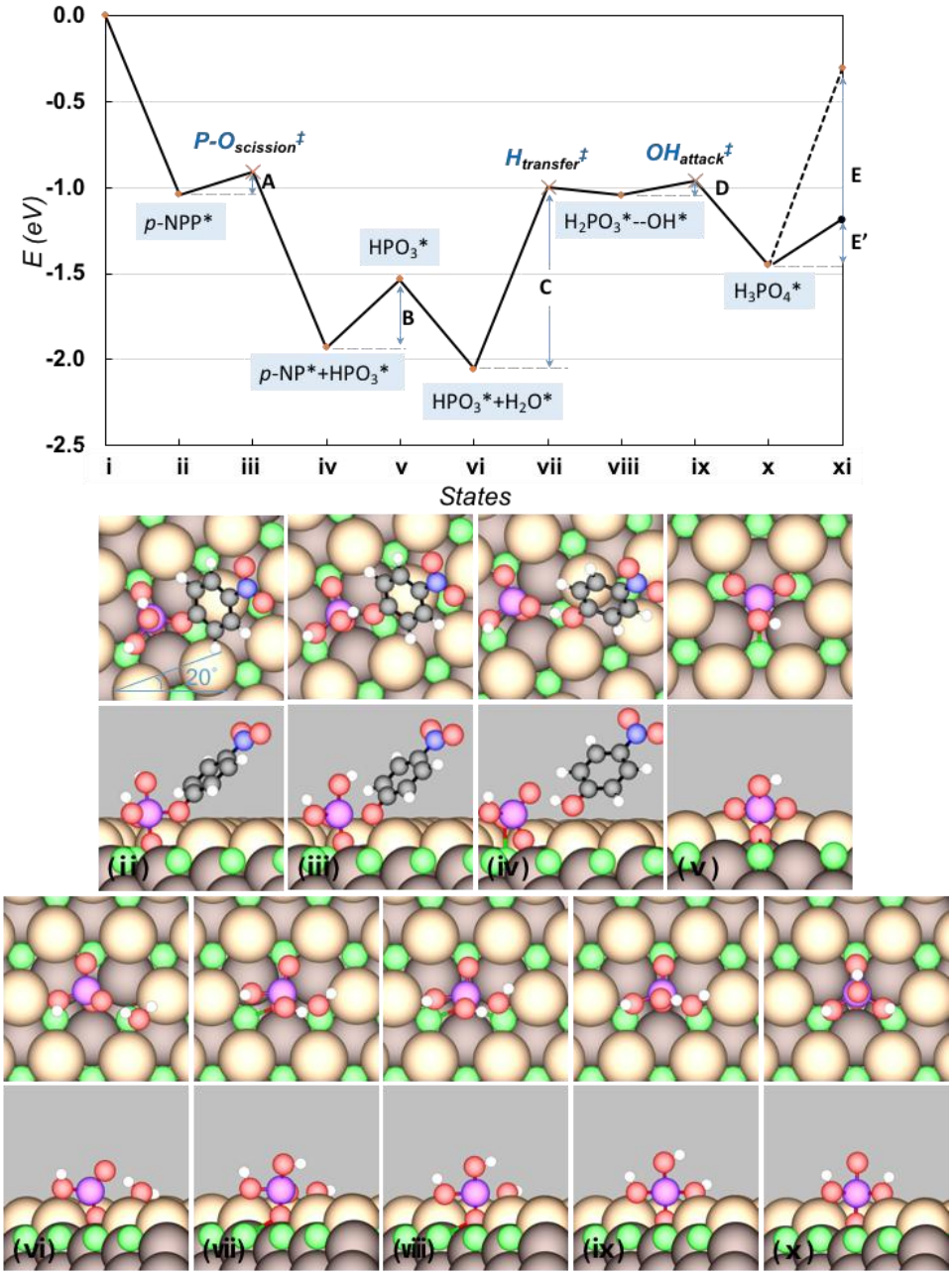

Figure 3. DFT-calculated minimum-energy reaction energy profile (not ZPE-corrected; entire path at zero magnetic moment) for the proposed dephosphorylation mechanism for *p*-NPP (including hydration of HPO_3) on CeO_2(111). Transition states are labeled by "‡". Surface adsorbed species are labeled by "*". *p*-NPP, H_2O, *p*-NP, and H_3PO_4 are treated as gas-phase molecules in States (i), (i)-(v), (v)-(xi) and (xi), respectively. Labeled activation or desorption processes are: A: P-O ester bond scission, E_a = 0.13 eV; B: *p*-NP desorption to gas phase, ΔE_{des} = 0.41 eV; C: H transfer, E_a = 1.05 eV; D: OH attack, E_a = 0.09 eV; E: H_3PO_4 desorption to gas phase, ΔE_{des} = 1.15 eV; E': H_3PO_4 desorption to aqueous phase, ΔE_{des} = 0.28 eV. Structures for states in the energy profile are shown in top and side views below the profile, the coordinates of which are reported in Supplemental Information. View is rotated by 40° counterclockwise from panel (iv) to (v), and by 60° clockwise from (v) to (vi). Color code: green=Ce, light brown=surface O_{latt}, dark brown=subsurface O_{latt}, red=O, violet=P, black=C, blue=N, and white=H.

To close the catalytic cycle, the HPO_3 group needs to be hydrated and desorb as H_3PO_4. We explored the direct addition of a water molecule to HPO_3 and found it to be very endothermic with a reaction energy in excess of 2 eV. Instead, hydration preferentially takes place in a step-wise mechanism (**Figure 3**). The minimum-energy pathway begins with a water molecule transferring a H atom to the axial O of phosphate, which has lost a H atom in the previous alcohol formation step. This hydrogen transfer step has an activation barrier of 1.05 eV (1.04 eV ZPE-corrected). The remaining hydroxyl group is now located at a distance of 1.831 Å between the P and O atoms in the intermediate state (**Figure 3viii**). The next step, OH attack forming H_3PO_4, is very facile with an activation energy of only 0.09 eV (0.06 eV ZPE-corrected). The desorption of H_3PO_4 is endothermic by 1.15 eV (1.07 eV ZPE-corrected). Thus, our calculations show that the hydration of HPO_3 and the desorption of H_3PO_4 are both rate-limiting steps in the overall dephosphorylation process *in vacuo*, with activation energies of ca. 1.1 eV.

Alternatively, we have investigated a stepwise hydration mechanism that begins with water dissociation on the surface, followed by OH attack before H transfer. The corresponding reaction energy profile is shown in **Figure 4**. The small barrier to water dissociation (0.32 eV, or 0.21 eV ZPE-corrected) is consistent with prior experimental [47] and theoretical [48-50] work that reported water dissociation to be very facile and reversible on CeO_2(111). The diffusion of a surface OH group, which positions it following water splitting for attack of the P center, is very facile with a diffusion barrier of ca. 0.1 eV, and so it is kinetically insignificant and therefore neglected from **Figure 4**. The OH attack step itself has an activation energy of 0.90 eV (0.92 eV ZPE-corrected), which results in a H_2PO_4 group. The remaining H atom is transferred from the

surface to the H_2PO_4 group with an activation energy of 0.61 eV (0.50 eV ZPE-corrected). Thus the total energetic barrier that HPO_3 hydration needs to overcome (i.e. between States vi and ix in Figures 3 and 4) is practically identical for both mechanisms (1.08 vs. 1.15 eV, or 1.08 vs. 1.14 eV ZPE-corrected). We conclude that within the accuracy of DFT it is kinetically equivalent whether OH attack occurs before or after H transfer, at least *in vacuo*.

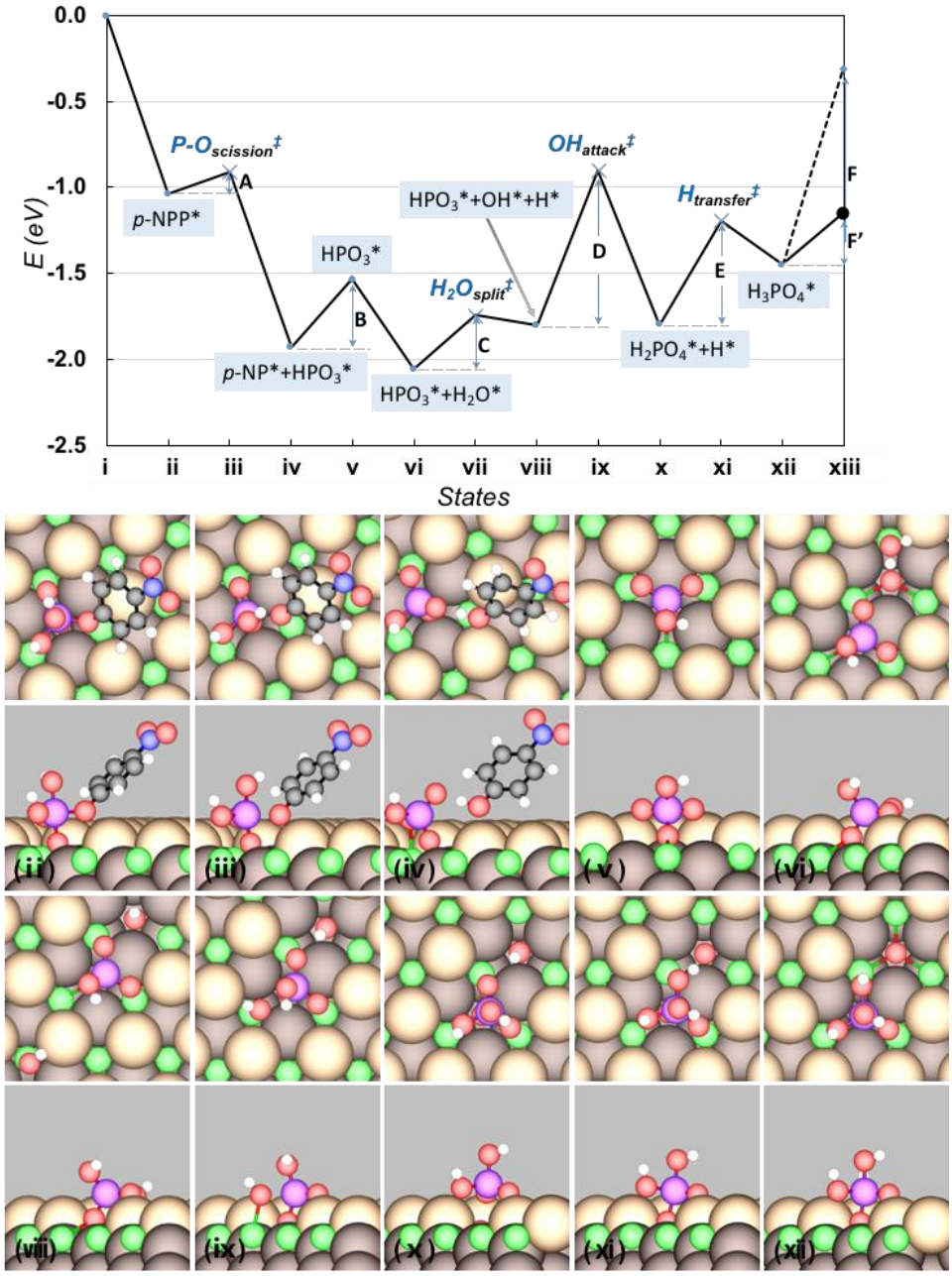

Figure 4. DFT-calculated minimum-energy reaction energy profile (not ZPE-corrected; entire path at zero magnetic moment) for the proposed dephosphorylation mechanism for *p*-NPP (including the alternate HPO_3 hydration mechanism) on $CeO_2(111)$. Transition states are labeled by "‡". Surface adsorbed species are labeled by "*". *p*-NPP, H_2O, *p*-NP and H_3PO_4 are treated as gas phase molecules in States (i), (i)-(v), (v)-(xiii), and (xiii), respectively. Labeled activation or desorption processes are: A: P-O ester bond scission, E_a = 0.13 eV; B: *p*-NP desorption to gas phase, ΔE_{des} = 0.41 eV; C: water splitting, E_a = 0.32 eV; D: OH attack, E_a = 0.90 eV; E: H transfer, E_a = 0.61 eV; F: H_3PO_4 desorption to gas phase, ΔE_{des} = 1.15 eV; F': H_3PO_4 desorption to aqueous phase, ΔE_{des} = 0.28 eV. Structures for states in the energy profile are shown in top and side views below the profile, the coordinates of which are reported in Supplemental Information. View is rotated by 40° counterclockwise from panel (iv) to (v), by 60° clockwise from (v) to (vi). Color code: green=Ce, light brown=surface O_{latt}, dark brown=subsurface O_{latt}, red=O, violet=P, black=C, blue=N, and white=H.

Experimentally, Manto et al. have reported the apparent activation energies to be 36.6±1.2, 76.5±1.9, 82.0±3.6, and 105.4±2.9 kJ/mol (100 kJ/mol ≈ 1 eV) for the nanospheres, nano-octahedra (which primarily expose (111) facets), nanorods, and nanocubes, respectively, in comparison to 57.4±2.7 kJ/mol for commercial CeO_2 powder [13]. While our DFT-calculated activation energies based on the rate-limiting steps are ca. 0.3 eV higher than the apparent activation energy corresponding to CeO_2(111), such a direct comparison is not meaningful due to potential concentration effects (e.g. reactant/product concentrations in solution were changing during experiment), coverage effects (surface site competition and lateral interaction are not considered here), as well as solvation effects. Solvation is expected to make the desorption of both the alcohol and phosphoric acid (or their deprotonated forms) much easier because they are well solvated by water [51, 52], so phosphate desorption may no longer be rate-limiting in aqueous phase. This can be seen in Figures 3 and 4, where we have indicated the solvation energy for molecular *p*-NPP in water calculated using an implicit solvent model [44]. We expect the species adsorbed on the ceria surface to also be partially solvated so that the promotional effect of solvation on desorption would be somewhat smaller than depicted. Presently the solvent model cannot be applied to the surface species on ceria due to problems in its implementation. Nonetheless, it is clear that the binding strengths, and thus the corresponding desorption barriers, of these species would be reduced at a water-ceria interface. In addition, there is theoretical evidence in the literature that solvation by water can stabilize the transition states of the formation of polarized bonds by a few tenths of an eV [53, 54], which suggests that the hydration of the phosphate group should occur at more appreciable rates at ambient conditions than the as-calculated activation barrier of ca. 1.1 eV would suggest. Furthermore, Manto et al. have shown that the apparent activation energy of *p*-NPP dephosphorylation can be

correlated to the surface density of oxygen vacancies [13], which suggests that the reaction mechanism may be different when *p*-NPP interacts with an oxygen vacancy, a surface element that is not considered in this study. Detailed microkinetic modeling accounting for adsorption/desorption, coverage and solvation effects, and varying extent of reduction in ceria will be attempted in the future to better validate our mechanistic model.

3.3 Adsorption and dephosphorylation of MP

The minimum-energy molecular adsorption state of neutral methyl phosphate (MP) has a similar configuration (**Figure 2b**) to that of *p*-NPP. Its formation is likewise found to be non-activated, just like for *p*-NPP. As can be seen in **Table 1**, the strength of the P-O_{latt} bond is nearly identical for *p*-NPP, MP, and H_3PO_4, suggesting that the P-O_{latt} bond is little affected by substitution of the acidic hydrogen by an organic group.

The P-O ester bond scission in MP occurs in a similar manner (see **Figure 5**) and produces HPO_3 and methanol in one step, and it has a noticeably higher activation energy of 0.50 eV (0.43 eV ZPE-corrected) than in *p*-NPP. After the formation and desorption of methanol, the hydration of the remaining HPO_3 group is identical to that described above. Overall, even though the methoxy group affects the activation energy of the P-O ester bond, the hydration of the phosphate group remains rate-limiting. We note that P-OCH_3 bond scission in a similar compound, dimethyl methylphosphonate (DMMP), has been reported to occur between 200 and 400 K on CeO_2(111), with which the small activation energy for P-OCH_3 bond scission in MP is in line [23]. It is worth mentioning that DMMP has been frequently studied as a proxy for certain chemical warfare agents, and what its reactivity has in common on a variety of solids under gas phase [22, 24-26] is P-OCH_3 bond scission under mild conditions but hindered removal of the remaining methylphosphonic acid group due to strong adsorption. This pattern is

similar to the dephosphorylation of *p*-NPP and MP that we are reporting herein, i.e. facile P-O ester bond scission but hindered removal of the phosphate group, in the absence of solvation effects.

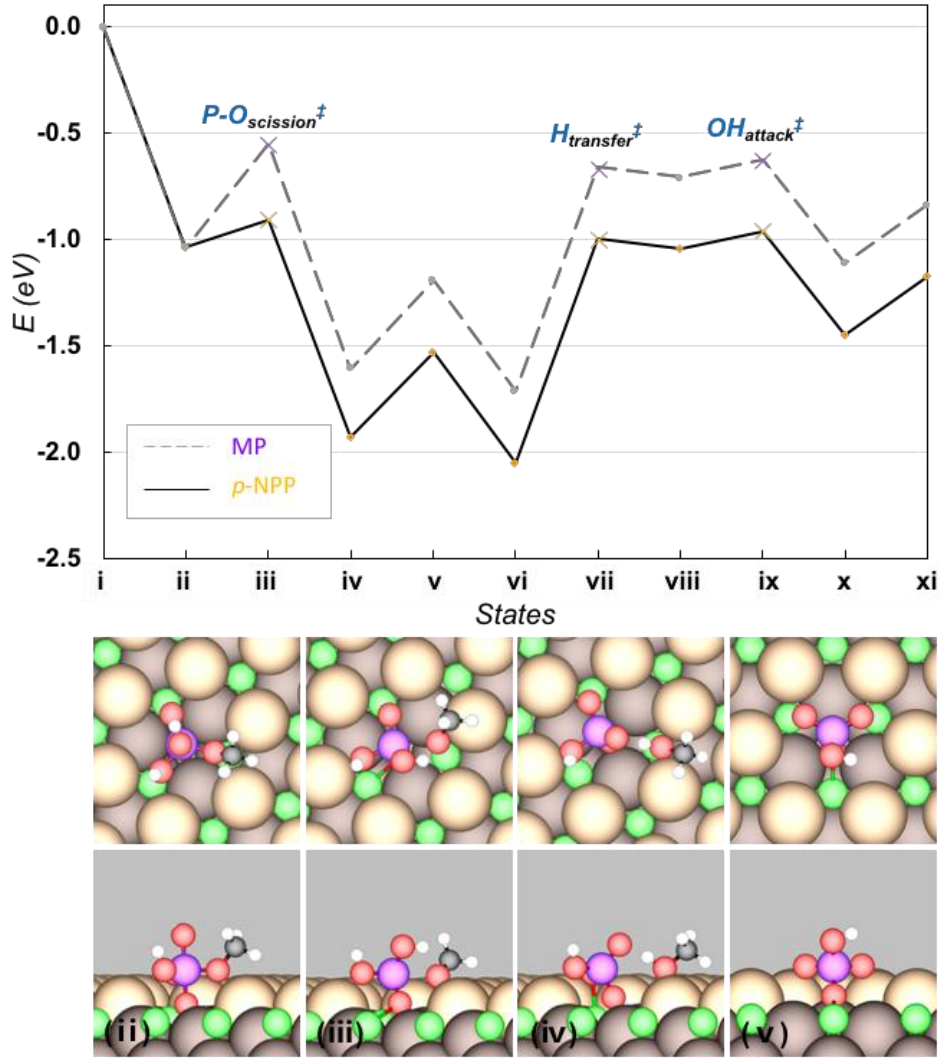

Figure 5. DFT-calculated minimum-energy reaction energy profiles (not ZPE-corrected; entire path at zero magnetic moment) for the proposed dephosphorylation mechanism for MP (dash line) and *p*-NPP (solid line) on CeO_2(111). Structures unique to the dephosphorylation of MP are shown in top and side views below the profile, the coordinates of which are reported in Supplemental Information. View is rotated by 40° counterclockwise from panel (iv) to (v). Color code: green=Ce, light brown=surface O_{latt}, dark brown=subsurface O_{latt}, red=O, violet=P, black=C, and white=H. Solvation energy of H_3PO_4 in water has been applied to the desorption energy in the final state (xi).

3.4 Comparison of hydrolysis mechanisms and the role of leaving group

Hydrolysis of phosphate esters in water has been extensively studied theoretically [15-21]. In general, as suggested by Warshel and coworkers [16-20], based on potential energy surfaces parameterized by two characteristic P-O bond distances (i.e., d(P-O_{NU}) and d(P-O_{LG}), where O_{NU} refers to the O atom of the nucleophile (i.e. water), and O_{LG} refers to the O atom of the leaving group), the hydrolysis mechanisms of phosphate monoesters in water fall into three major categories: 1) the associative type, where the nucleophilic attack occurs first forming an intermediate complex with a pentavalent P center, followed by a second transition state corresponding to the P-O_{LG} bond scission; 2) the dissociative type, where the leaving group departs before the nucleophilic attack and formation of the P-O_{NU} bond; 3) the concerted type, where the reaction proceeds via a single transition state with both P-O_{NU} and P-O_{LG} bonding characters [17, 21]. The mechanistic preference appears to be influenced by the pK_a of the leaving group in water, with poor leaving groups (high pK_a) favoring associative mechanisms and good leaving groups (lower pK_a) favoring dissociative mechanisms [17, 21]. Among others, Florián et al. used Hartree-Fock (HF) and second-order Møller-Plesset perturbation theory (MP2) together with the Langevin dipoles (LD) model as well as the polarized-continuum model (PCM) to study the hydrolysis of neutral, mono-anionic, and di-anionic MP [16]. A more recent example is the work of Duarte et al., who used the M06-2X and ωB97X-D density functionals and a mixture of implicit/explicit solvent models to investigate the hydrolysis of the di-anions of several aryl phosphate monoesters as well as MP in water [21]. The hydrolysis of the neutral MP is found to preferentially proceed via an associative mechanism, while the associative and dissociative mechanisms are competitive for the mono-anionic and the di-anionic MP [16]. The highest activation free energies for the hydrolysis of neutral, mono-anionic, and di-anionic MP

were reported by Florián et al. to be 1.52, 1.73, and 1.65 eV in MP2+LD, and by Duarte et al. to be 1.54 eV in M06-2X and 1.74 eV in ωB97X-D for di-anionic MP. On the other hand, Duarte et al. found di-anionic *p*-NPP to prefer a concerted mechanism with a single barrier calculated to be 1.18 eV in M06-2X and 1.08 eV in ωB97X-D [21], and they reported a threshold pK_a value of ca. 12, below which the hydrolysis of a phosphate monoester di-anion prefers a concerted mechanism, and above which an associative mechanism would prevail [21]. The pK_a of several alkoxide leaving groups are listed in **Table 2**. In particular, the pK_a of *para*-nitrophenoxide and methoxide in water is 7.1 and 15.5, respectively.

A $CeO_2(111)$ surface presents a large number of exposed O_{latt} atoms that can act as nucleophiles to coordinate to the P atoms in the phosphates, as well as Lewis bases to accept protons from the phosphates or from water. As mentioned above, an optimal pentavalent structure for model phosphate monoesters is formed on $CeO_2(111)$ without any activation energy. Here the P center is activated prior to P-O bond scission by a nucleophilic attack, although it is done by ceria and not water. Then the P-O bond preferentially dissociates, followed by the hydration of the remaining phosphate group and its desorption as H_3PO_4, each of which has an activation energy of ca. 1.1 eV. Thus the surface-assisted dephosphorylation process on $CeO_2(111)$ possesses features of both associative and dissociative mechanisms in aqueous solution but does not strictly conform to either.

Although P-O ester bond scission is not rate-limiting in the dephosphorylation of *p*-NPP and MP on $CeO_2(111)$, it could be significant in other phosphate monoesters. Thus we explored ester bond scission in four additional neutral organic phosphate monoesters on $CeO_2(111)$, including *para*-chlorophenyl phosphate (*p*-ClPP), phenyl phosphate (PP), 2-pyridyl phosphate (2-py-P), and chloro-methyl phosphate (Cl-MP). The minimum-energy gas-phase geometries for

all the phosphates are shown in **Figure 1**, and the minimum-energy geometries for the molecular adsorption of the four additional phosphates and the corresponding P-O ester bond scission transition states on CeO_2(111) are shown in **Figure 6**, with additional molecular properties listed in **Table 2**. As shown in **Figure 7**, a linear relation with a slope of 0.66 results, which relates the energy of the transition state of P-O ester bond scission to the energies of the dissociated moieties (alkoxide and H_2PO_3) on CeO_2(111). The correlation is not particularly strong possibly because the P-O bonds in most of these phosphate monoesters are significantly weakened on CeO_2(111), causing the activation energies of the P-O ester bond scission fall within DFT margins of error and thus making the accurate capture of the transition states challenging. Nonetheless, the energies of the dissociated moieties may still be used to provide quick estimates for the energies of the transition states of P-O ester bond scission and therefore the corresponding P-O ester bond scission barriers for other phosphate monoesters. As summarized in **Table 3**, the activation energies for activating the P-O ester bonds in these phosphate monoesters on CeO_2(111) are also closely related to the corresponding P-O ester bond energies in gas phase, and they are all significantly lower than the activation energies for phosphate hydration and desorption *in vacuo*.

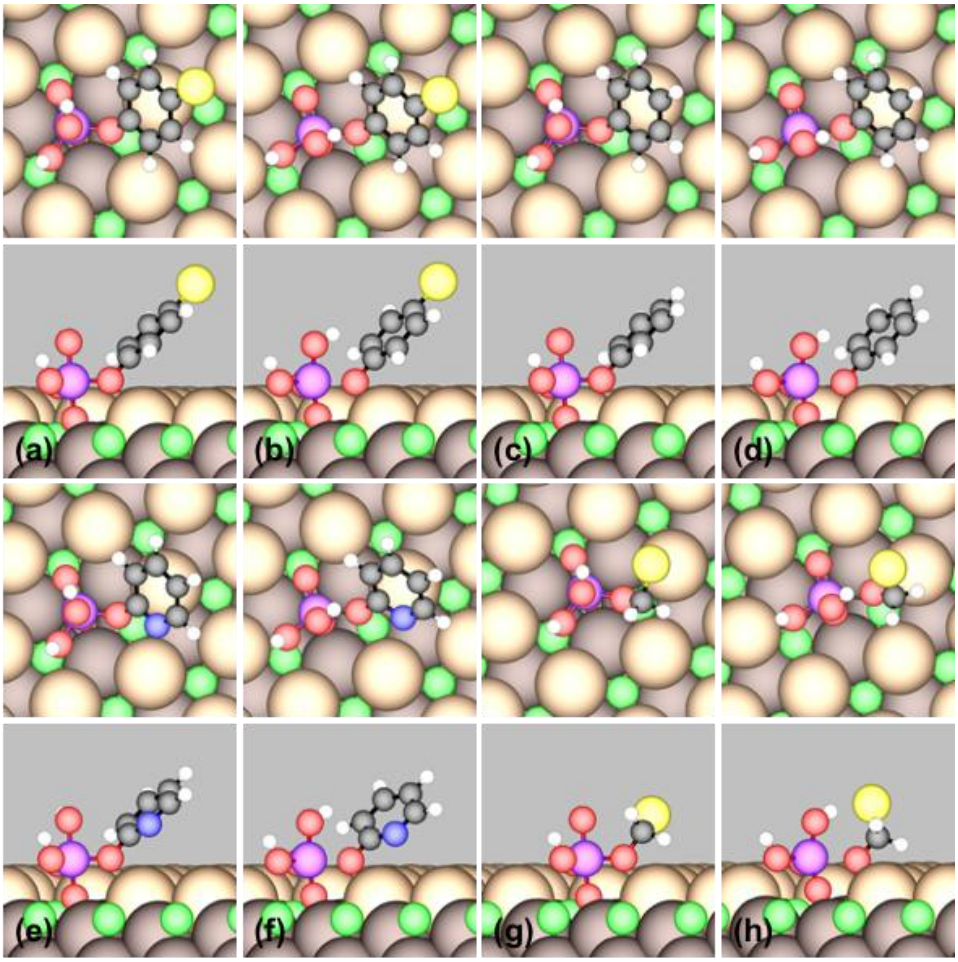

Figure 6. Top (top panels) and side (bottom panels) views of DFT-calculated minimum-energy geometries for: (a) molecular adsorption state and (b) corresponding transition state for P-O ester bond scission on CeO_2(111) (same below) for *p*-ClPP; (c) molecular adsorption and (d) transition state for PP; (e) molecular adsorption and (f) transition state for 2-py-P; (g) molecular adsorption and (h) transition state for Cl-MP. The coordinates of these structures are reported in Supplemental Information. Color code: green=Ce, light brown=surface O_{latt},, dark brown= subsurface O_{latt}, red=O, violet=P, black=C, blue=N, white=H, and yellow=Cl.

Table 2. DFT-calculated minimum adsorption energies (ΔE_{ads}, in eV) and corresponding P-O bond lengths (d(P-O_{latt}), in Å; ester bond d(P-O), in Å; gas-phase ester bond (d(P-O)^{gas}, in Å) included for comparison), and magnetic moments (m.m., in μ_B).

Adsorbate	ΔE_{ads}	pK_a[†]	d(P-O_{latt})	d(P-O)	d(P-O)^{gas}	e(P)	e(O_{latt})	m.m.
p-NPP	-1.04	–	1.687	1.706	1.619	+3.51	-1.34	0
MP	-1.04	–	1.701	1.670	1.599	+3.44	-1.31	0
p-ClPP	-0.99	–	1.692	1.703	1.606	+3.47	-1.32	0
PP	-0.98	–	1.694	1.697	1.602	+3.47	-1.32	0
2-py-P	-0.65	–	1.690	1.694	1.666	+3.46	-1.33	0
Cl-MP	-1.03	–	1.691	1.707	1.640	+3.45	-1.32	0
p-NP_x	-0.22	7.1	–	–	–	–	–	1
CH_3O	-0.63	15.5	–	–	–	–	–	1
p-ClP_x	-0.09	9.4	–	–	–	–	–	1
phenoxy	-0.23	10.0	–	–	–	–	–	1
2-oxopyridine	-0.30	n/a	–	–	–	–	–	1
$ClCH_2O$	-0.58	n/a	–	–	–	–	–	1

Adsorption energies are not ZPE-corrected. Adsorbate coverage is 1/9 ML. O_{latt} refers to the surface O atom that forms a bond with P.

[†] pK_a values of *p*-NP_x, CH_3O, *p*-ClP_x, and phenoxy are obtained from Ref. [21].

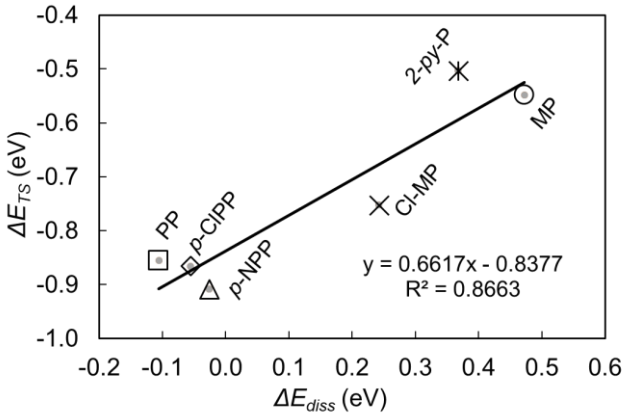

Figure 7. Transition state scaling relation between the adsorption energies of the transition states for P-O ester bond scission of model phosphate monoesters and the adsorption energies of the dissociated fragments (alkoxide and H_2PO_3, at infinite separation) on CeO_2(111). The energies are referenced to the corresponding neutral gas-phase phosphate monoesters.

Table 3. Gas-phase P-O ester bond energies ($E_b^{P\text{-}O}$, in eV), corresponding activation energies for P-O ester bond scission on CeO_2(111) (E_a and zero-point energy corrected value E_a^{ZPE}, in eV), energies of transition state relative to gas phase molecule (ΔE_{TS}, in eV), and energies of dissociated moieties at infinite separation relative to gas phase molecule (ΔE_{diss}, in eV) for model phosphate monoesters on CeO_2(111)

Species	$E_b^{P\text{-}O}$	E_a	E_a^{ZPE}	ΔE_{TS}	ΔE_{diss}
p-NPP	3.54	0.13	0.12	-0.91	-0.03
MP	4.45	0.50	0.43	-0.55	0.47
p-ClPP	3.37	0.13	0.11	-0.87	-0.06
PP	3.47	0.13	0.11	-0.86	-0.11
2-py-P	4.01	0.14	0.13	-0.50	0.37
Cl-MP	4.17	0.28	0.23	-0.75	0.24

The potential significance of ceria as a catalyst for dephosphorylation is suggested by **Figure 7** and **Table 3**. Ceria can readily weaken the P-O ester bond to the extent that P-O ester bond scission is kinetically insignificant for a range of phosphate monoesters compared to phosphate hydration and desorption, and the proposed surface-assisted dephosphorylation mechanism should apply to all of the phosphate monoesters. In other words, our calculations predict that the intrinsic catalytic activity of CeO_2(111) toward dephosphorylation should be independent of the alkoxide group. This is true even for MP, in which methoxy is a poor leaving group that causes the hydrolysis of MP to have a significant activation energy in aqueous solution. Thus ceria and ceria related materials may have the potential to be developed into environmental phosphorus recovery and phosphate detoxification technologies for a variety of organic phosphates. Whether ceria does have significant catalytic dephosphorylation activity toward other types of organophosphates, such as phosphate diesters and triesters [55] and phosphonates and phosphorothioates (notable examples of which include chlorpyrifos and glyphosate), will be the subject of our future studies.

4 Conclusions

The dephosphorylation of two model phosphate monoesters, neutral *para*-nitrophenyl phosphate and methyl phosphate, on CeO_2(111) has been investigated theoretically *in vacuo* using self-consistent, periodic DFT+U calculations (GGA-PW91). A surface-assisted hydrolysis mechanism is proposed, which involves the barrier-less activation of the phosphates by adsorption on CeO_2(111) and formation of a P-O_{latt} bond, facile dissociation of the P-O ester bond, hydration of the remaining HPO_3 group, and desorption of H_3PO_4. The last two steps are found to be rate-limiting *in vacuo* with activation energies of ca. 1.1 eV, both of which are expected to be reduced by solvation effects. P-O ester bond scission in several other phosphate monoesters has been investigated and is found consistently to have low activation energies, in contrast to the large bond energy of the P-O ester bond in the isolated molecules. The overall catalytic performance of CeO_2(111) in dephosphorylation process is therefore predicted to be independent of the nature of the alkoxide group. Our findings suggest that ceria can be catalytically active toward the dephosphorylation of organic phosphates in general under ambient conditions and may serve as the core of technologies for the recycling of phosphorus from, and detoxification of, organic phosphates in the environment.

Acknowledgements

This work was supported by the U.S. National Science Foundation under Grant #CHE-1664984, and has used high performance computational resources provided by Louisiana State University (http://hpc.lsu.edu), by the Center for Nanophase Materials Sciences, which is a DOE Office of Science User Facility, and by the National Energy Research Scientific Computing Center, which is supported by the Office of Science of US-DOE under Contract No. DE-AC02-05CH11231.

References

[1] D. Cordell, J.O. Drangert, S. White, Global. Environ. Chang. 19 (2009) 292-305.
[2] L. Reijnders, Resour. Conserv. Recy. 93 (2014) 32-49.
[3] S.R. Carpenter, P. Natl. Acad. Sci. USA. 105 (2008) 11039-11040.
[4] S.A. Parsons, J.A. Smith, Elements. 4 (2008) 109-112.
[5] B.K. Mayer, L.A. Baker, T.H. Boyer, P. Drechsel, M. Gifford, M.A. Hanjra, P. Parameswaran, J. Stoltzfus, P. Westerhoff, B.E. Rittmann, Environ. Sci. Technol. 50 (2016) 6606-6620.
[6] V.H. Freed, C.T. Chiou, D.W. Schmedding, J. Agr. Food. Chem. 27 (1979) 706-708.
[7] C. Lad, N.H. Williams, R. Wolfenden, P. Natl. Acad. Sci. USA. 100 (2003) 5607-5610.
[8] B.K. Singh, A. Walker, Fems. Microbiol. Rev. 30 (2006) 428-471.
[9] F. Tan, Y. Zhang, J. Wang, J. Wei, Y. Cai, X. Qian, J. Mass. Spectrom. 43 (2008) 628-632.
[10] M.H. Kuchma, C.B. Komanski, J. Colon, A. Teblum, A.E. Masunov, B. Alvarado, S. Babu, S. Seal, J. Summy, C.H. Baker, Nanomed-Nanotechnol. 6 (2010) 738-744.
[11] P. Janos, P. Kuran, M. Kormunda, V. Stengl, T.M. Grygar, M. Dosek, M. Stastny, J. Ederer, V. Pilarova, L. Vrtoch, J. Rare. Earth. 32 (2014) 360-370.
[12] P. Janos, P. Kuran, V. Pilarova, J. Trogl, M. Stastny, O. Pelant, J. Henych, S. Bakardjieva, O. Zivotsky, M. Kormunda, K. Mazanec, M. Skoumal, Chem. Eng. J. 262 (2015) 747-755.
[13] M.J. Manto, P.F. Xie, C. Wang, ACS. Catal. 7 (2017) 1931-1938.
[14] J.K. Lassila, J.G. Zalatan, D. Herschlag, Annul. Rev. Biochem. 80 (2011) 669-702.
[15] J. Florian, A. Warshel, J. Am. Chem. Soc. 119 (1997) 5473-5474.
[16] J. Florian, A. Warshel, J. Phys. Chem. B. 102 (1998) 719-734.
[17] M. Klähn, E. Rosta, A. Warshel, J. Am. Chem. Soc. 128 (2006) 15310-15323.
[18] S.C.L. Kamerlin, N.H. Williams, A. Warshel, J. Org. Chem. 73 (2008) 6960-6969.
[19] B.R. Prasad, N.V. Plotnikov, A. Warshel, J. Phys. Chem. B. 117 (2013) 153-163.
[20] S.C.L. Kamerlin, P.K. Sharma, R.B. Prasad, A. Warshel, Q. Rev. Biophys. 46 (2013) 1-132.
[21] F. Duarte, A. Barrozo, J. Aqvist, N.H. Williams, S.C.L. Kamerlin, J. Am. Chem. Soc. 138 (2016) 10664-10673.
[22] C.N. Rusu, J.T. Yates, J. Phys. Chem. B. 104 (2000) 12292-12298.
[23] D.A. Chen, J.S. Ratliff, X. Hu, W.O. Gordon, S.D. Senanayake, D.R. Mullins, Surf. Sci. 604 (2010) 574-587.
[24] G. Wang, C. Sharp, A.M. Plonka, Q. Wang, A.I. Frenkel, W. Guo, C. Hill, C. Smith, J. Kollar, D. Troya, J.R. Morris, J. Phys. Chem. C. 121 (2017) 11261-11272.
[25] Q. Wang, R.C. Chapleski, A.M. Plonka, W.O. Gordon, W. Guo, T.-D. Nguyen-Phan, C.H. Sharp, N.S. Marinkovic, S.D. Senanayake, J.R. Morris, C.L. Hill, D. Troya, A.I. Frenkel, Sci. Rep-UK. 7 (2017) 773.
[26] L. Trotochaud, R. Tsyshevsky, S. Holdren, K. Fears, A.R. Head, Y. Yu, O. Karslıoğlu, S. Pletincx, B. Eichhorn, J. Owrutsky, J. Long, M. Zachariah, M.M. Kuklja, H. Bluhm, Chem. Mater. 29 (2017) 7483-7496.
[27] C.A. Bunton, D.R. Llewellyn, K.G. Oldham, C.A. Vernon, J. Chem. Soc. 0 (1958) 3574-3587.
[28] K.D. Kwon, J.D. Kubicki, Langmuir. 20 (2004) 9249-9254.
[29] G. Kresse, J. Furthmuller, Phys. Rev. B. 54 (1996) 11169-11186.
[30] J.P. Perdew, J. Chevary, S. Vosko, K.A. Jackson, M.R. Pederson, D. Singh, C. Fiolhais, Phys. Rev. B. 46 (1992) 6671.

[31] G. Kresse, D. Joubert, Phys. Rev. B. 59 (1999) 1758-1775.
[32] J. Neugebauer, M. Scheffler, Phys. Rev. B. 46 (1992) 16067.
[33] H.J. Monkhorst, J.D. Pack, Phys. Rev. B. 13 (1976) 5188-5192.
[34] G. Henkelman, B.P. Uberuaga, H. Jónsson, J. Chem. Phys. 113 (2000) 9901-9904.
[35] S. Smidstrup, A. Pedersen, K. Stokbro, H. Jonsson, J. Chem. Phys. 140 (2014) 214106.
[36] G. Henkelman, H. Jónsson, J. Chem. Phys. 111 (1999) 7010-7022.
[37] A. Heyden, A.T. Bell, F.J. Keil, J. Chem. Phys. 123 (2005) 224101.
[38] S.L. Dudarev, G.A. Botton, S.Y. Savrasov, C.J. Humphreys, A.P. Sutton, Phys. Rev. B. 57 (1998) 1505-1509.
[39] G. Kresse, P. Blaha, J.L.F. Da Silva, M.V. Ganduglia-Pirovano, Phys. Rev. B. 72 (2005) 237101.
[40] F.C. Calaza, Y. Xu, D.R. Mullins, S.H. Overbury, J. Am. Chem. Soc. 134 (2012) 18034-18045.
[41] F.C. Calaza, T.L. Chen, D.R. Mullins, Y. Xu, S.H. Overbury, Catal. Today. 253 (2015) 65-76.
[42] C. Zhao, Y. Xu, Top. Catal. 60 (2017) 446-458.
[43] J. Paier, C. Penschke, J. Sauer, Chem. Rev. 113 (2013) 3949-3985.
[44] K. Mathew, R. Sundararaman, K. Letchworth-Weaver, T.A. Arias, R.G. Hennig, J. Chem. Phys. 140 (2014) 8.
[45] W. Tang, E. Sanville, G. Henkelman, J. Phys-Condens. Mat. 21 (2009) 084204.
[46] K. Momma, F. Izumi, J. Appl. Crystallogr. 41 (2008) 653-658.
[47] D.R. Mullins, P.M. Albrecht, T.L. Chen, F.C. Calaza, M.D. Biegalski, H.M. Christen, S.H. Overbury, J. Phys. Chem. C. 116 (2012) 19419-19428.
[48] D. Marrocchelli, B. Yildiz, J. Phys. Chem. C. 116 (2012) 2411-2424.
[49] D. Fernández-Torre, K. Kośmider, J. Carrasco, M.V. Ganduglia-Pirovano, R. Pérez, J. Phys. Chem. C. 116 (2012) 13584-13593.
[50] M.F. Camellone, F.R. Negreiros, L. Szabová, Y. Tateyama, S. Fabris, J. Am. Chem. Soc. 138 (2016) 11560-11567.
[51] Y. Marcus, Ion properties, Marcel Dekker, New York, 1997.
[52] M. Śmiechowski, J. Mol. Struct. 924 (2009) 170-174.
[53] B.N. Zope, D.D. Hibbitts, M. Neurock, R.J. Davis, Science. 330 (2010) 74-78.
[54] X. Nie, M.R. Esopi, M.J. Janik, A. Asthagiri, Angew. Chem. Int. Edit. 52 (2013) 2459-2462.
[55] A.J. Kirby, F. Nome, Accounts. Chem. Res. 48 (2015) 1806-1814.

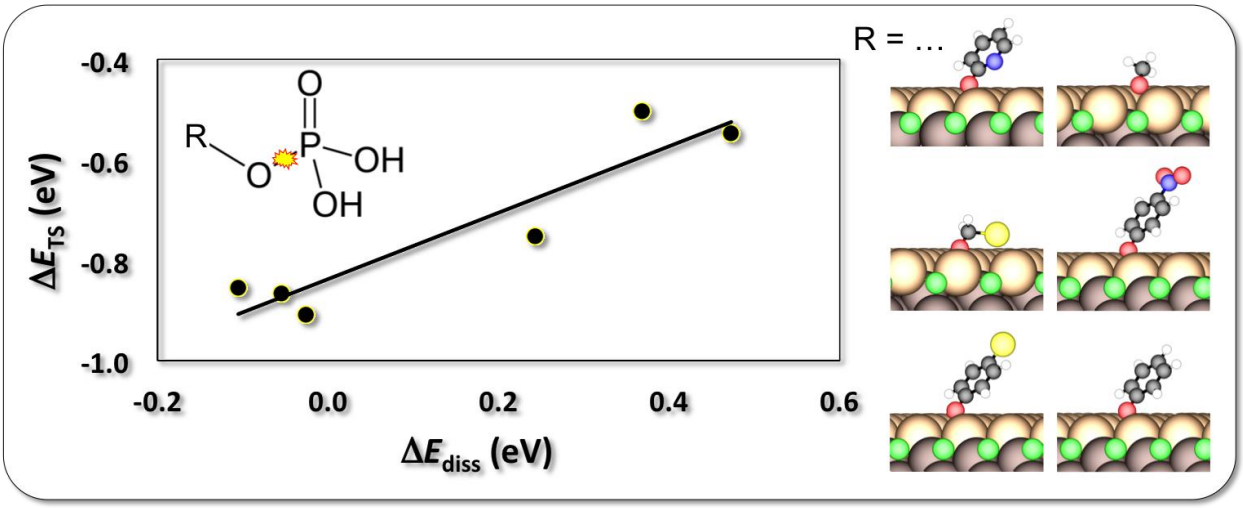
-0.4
-0.6
-0.8
-1.0
ΔE_{TS} (eV)
-0.2
0.0
0.2
0.4
0.6
ΔE_{diss} (eV)
O
R
O
P
OH
OH
R = …